

1  
2  
3  
4  
5  
6  
7  
8  
9  
10  
11  
12  
13  
14  
15  
16  
17  
18  
19  
20  
21  
22  
23

## A simple correction term to model infiltration in water-repellent soils

Majdi R. Abou Najm<sup>1,2,\*</sup>, Ryan D. Stewart<sup>3</sup>, Simone Di Prima<sup>4,5</sup>, and Laurent Lassabatere<sup>5</sup>

<sup>1</sup> Department of Land, Air and Water Resources, University of California, Davis, CA 95616, United States.

<sup>2</sup> John Muir Institute of the Environment, University of California, Davis, CA 95616, United States.

<sup>3</sup> School of Plant and Environmental Sciences, Virginia Polytechnic Institute and State University, Blacksburg, VA, United State.

<sup>4</sup> Department of Agricultural Sciences, University of Sassari, Viale Italia, 39, 07100 Sassari, Italy.

<sup>5</sup> Université de Lyon; UMR5023 Ecologie des Hydrosystèmes Naturels et Anthropisés, CNRS, ENTPE, Université Lyon 1, Vaulx-en-Velin, France.

\* Corresponding Author. E-mail: mabounajm@ucdavis.edu

### Key Points:

- We propose a simple correction term for infiltration models to characterize water repellency in infiltration models
- One hundred and sixty five infiltration experiments from three different ecosystems and levels of water repellencies were used to demonstrate model effectiveness
- The one parameter correction substantially reduced model error and reflected the changing rate of water repellency during infiltration

Citation: Abou Najm, M. R., Stewart, R. D., Di Prima, S., & Lassabatere, L. (2021). A simple correction term to model infiltration in water-repellent soils. *Water Resources Research*, 57, e2020WR028539. <https://doi.org/10.1029/2020WR028539>

Received 10 AUG 2020

Accepted 12 JAN 2021

24 **Abstract**

25 Soil water repellency can substantially alter hydrologic processes, particularly the ability of soils  
26 to infiltrate water. Water repellency often changes through time, making it difficult to simulate  
27 infiltration behaviors of water-repellent soils using standard models. Here, we propose a simple  
28 rate-based correction term that starts with a value of zero at the beginning of the infiltration  
29 process ( $t = 0$ ) and asymptotically approaches 1 as time increases, thus simulating decreasing soil  
30 water repellency through time. The correction term can be used with any model for infiltration  
31 rate. For this study we selected a simple two-term infiltration equation and then, using two  
32 datasets of infiltration measurements conducted in soils with varying water repellency, compared  
33 model error with versus without the added term. The correction substantially reduced model  
34 error, particularly in more repellent soils. At the same time, the rate constant parameter  
35 introduced in the new model may be useful to better understand dynamics of soil water  
36 repellency and to provide more consistent interpretations of hydraulic properties in water-  
37 repellent soils.

## 38 **Introduction**

39 Water repellency can form in soils under a wide spectrum of conditions, including deposition of  
40 resinous materials and exudates from vegetation (Lichner et al., 2018), vaporization and  
41 condensation of organic compounds during fires (DeBano et al., 1970), and presence of  
42 anthropogenic-derived chemicals such as petroleum products (Adams et al., 2008; Badin et al.,  
43 2008; Hewelke et al., 2018; Roy & McGill, 2000), wastewater (Arye et al., 2011) or other urban  
44 contaminants (Stavi & Rosenzweig, 2020). Soil water repellency can range from mild to severe,  
45 with the latter often considered to represent hydrophobic conditions. When present, soil water  
46 repellency affects many aspects of the hydrological cycle, including infiltration, surface runoff,  
47 and evaporation (Bauters et al., 2000; Doerr et al., 2006, p. 20; Ebel et al., 2012; Imeson et al.,  
48 1992; Mansell, 1970; Rye & Smettem, 2017). These effects can extend to watershed-scale  
49 responses, such as increased flooding and debris flows (Ebel et al., 2016; McGuire et al., 2018;  
50 Rengers et al., 2019).

51 Soil water repellency often diminishes or dissipates in the presence of liquid water (Dekker et al.,  
52 2001; Doerr & Thomas, 2000), meaning that infiltration can reduce water repellency through  
53 time. This interaction in turn often causes infiltration rates to gradually increase (J. Chen, Pangle,  
54 et al., 2020; Ebel et al., 2016; Robichaud, 2000). This dynamic process results in atypical  
55 infiltration behaviors, e.g., cumulative infiltration forming upwardly convex curves with time  
56 (Concialdi et al., 2020; Di Prima et al., 2017; Li et al., 2018). However, many studies continue to  
57 use standard equations, such as the two-term model first developed by Philip (1957), to simulate  
58 infiltration in fire-affected and other water-repellent soils (Ebel & Moody, 2020; McGuire et al.,  
59 2018; Moody et al., 2019). This approach can require extensive calibration (L. Chen, Berli, et al.,

60 2013), which often results in non-physical parameters, e.g., negative or null values for hydraulic  
61 conductivity (Di Prima et al., 2019).

62 Here, we propose a simple correction term  $(1 - e^{-\alpha_{WR}t})$  to modify models for infiltration rate.  
63 The correction term starts with a value of zero at the beginning of the infiltration experiment ( $t =$   
64 0) and asymptotically approaches 1 as time increases, thus simulating decreasing soil water  
65 repellency through time. Further, the correction only uses a single rate-constant parameter  
66 ( $\alpha_{WR}$ ), whose reciprocal reflects the time-scale of water repellency, and thus may be useful to  
67 characterize the duration of water repellency.

## 68 **Theory**

69 Water repellency often delays the start of infiltration and attenuates infiltration rates, particularly  
70 at the early times of rainfall or irrigation events. We model this response using an exponential  
71 scaling factor:

$$72 \quad i_{WR}(t) = i(t) (1 - e^{-\alpha_{WR}t}) \quad [1]$$

73 where  $i_{WR}(t)$  is the scaled infiltration rate [ $LT^{-1}$ ],  $i(t)$  is the unscaled infiltration rate (i.e., as  
74 modeled using a wide range of conventional equations of infiltration models that do not account  
75 for water repellency) [ $LT^{-1}$ ],  $t$  is the time elapsed since the start of the infiltration event [T], and  
76  $\alpha_{WR}$  is a newly introduced empirical soil parameter [ $T^{-1}$ ] that describes the rate of attenuation of  
77 infiltration rate.  $\alpha_{WR}$  can be considered to be a rate constant associated with change in water  
78 repellency through time. Here, we stress that Equation [1] is broadly defined and can be used  
79 with any infiltration model (short-term, steady state, one-dimensional, two-dimensional, or three-  
80 dimensional). We also consider that the correcting factor quantifies the effect of water repellency

81 at the soil surface without impacting processes in the soil, so that  $i(t)$  continues to be quantified  
82 in a regular way from the soil hydraulic properties (e.g., soil sorptivity and hydraulic  
83 conductivity). Such correction typically applies to fire-induced water repellency or factors that  
84 affect the soil mainly at surface (vegetation inputs).

85 We can also define a characteristic time for water repellency,  $t_{WR}$  [T], as:

$$86 \quad t_{WR} = \ln(2)/\alpha_{WR} \quad [2]$$

87 Based on Equation [2],  $t_{wr}$  represents the time at which the infiltration rate of the water-repellent  
88 soil is half that of the equivalent non-repellent soil, i.e.,  $i_{WR}(t)/i(t) = 0.5$ . In other words,  $t_{WR}$   
89 identifies the time at which the term  $(1 - e^{-\alpha_{WR}t}) = 0.5$ . We will use this concept to test the  
90 hypothesis that infiltration rates are affected for longer periods of time in soils with more severe  
91 water repellency.

92 To demonstrate the effectiveness of this method, we use a simple two-term infiltration model  
93 (Stewart & Abou Najm, 2018a; Vandervaere et al., 2020a, 2020b):

$$94 \quad I(t) = c_1 t^{1/2} + c_2 t \quad [3]$$

95 where  $c_1$  [ $LT^{-1/2}$ ] and  $c_2$  [ $L T^{-1}$ ] are constants specific to the soil type and initial and boundary  
96 conditions (e.g., ponding depth, ring geometry, initial water content). For example, in the one-  
97 dimensional Philip (1969) model for vertical infiltration,  $c_1$  is sorptivity ( $S$ ) [ $LT^{-1/2}$ ] and  $c_2$  is  $A$  [ $L$   
98  $T^{-1}$ ] (a term related to hydraulic conductivity).

99 The infiltration rate,  $i$  [ $L T^{-1}$ ], for the two-term model of Equation [3] is

$$100 \quad i(t) = \frac{c_1}{2\sqrt{t}} + c_2 \quad [4]$$

101  
102

103 Here we modify Equation [4] to account for water repellency,  $i_{WR}(t)$  [ $L T^{-1}$ ], as:

$$104 \quad i_{WR}(t) = i(t)(1 - e^{-\alpha_{WR}t}) = \left(\frac{c_1}{2\sqrt{t}} + c_2\right)(1 - e^{-\alpha_{WR}t}) \quad [5].$$

105 Cumulative infiltration,  $I_{WR}$  [L], is then found by integrating Equation [5] with respect to time:

$$106 \quad I_{WR}(t) = c_1\sqrt{t} - \frac{c_1\sqrt{\pi}}{2\sqrt{\alpha_{WR}}} \operatorname{erf}(\sqrt{\alpha_{WR}t}) + c_2t - \frac{c_2(1 - e^{-\alpha_{WR}t})}{\alpha_{WR}} \quad [6].$$

107 Equation [6] can be written as:

$$108 \quad I_{WR}(t) = c_1\sqrt{t} - \frac{c_1\sqrt{\pi}}{2\sqrt{\alpha_{WR}}} \left(1 - \frac{e^{-\alpha_{WR}t}}{\sqrt{\pi\alpha_{WR}t}} g(t)\right) + c_2t - \frac{c_2(1 - e^{-\alpha_{WR}t})}{\alpha_{WR}} \quad [7]$$

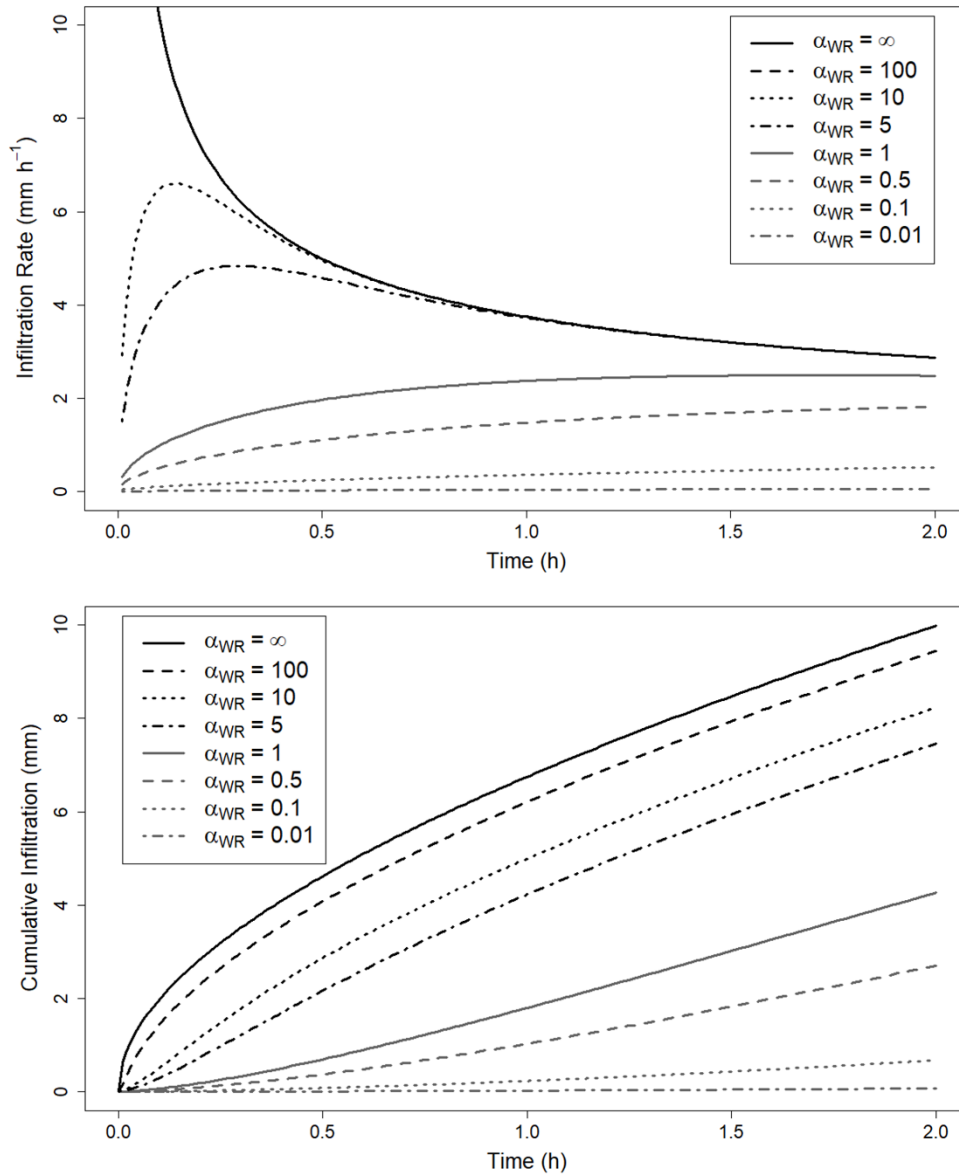
109 where  $g(t)$  is approximated as (Winitzki 2003):

$$110 \quad g(t) \approx \frac{\sqrt{\pi\alpha_{WR}t} + (\pi - 2)\alpha_{WR}t}{1 + \sqrt{\pi\alpha_{WR}t} + (\pi - 2)\alpha_{WR}t} \quad [8].$$

111 Combining Equations [7] and [8]:

$$112 \quad I_{WR}(t) \approx c_1\sqrt{t} + c_2t - \frac{c_1\sqrt{\pi}}{2\sqrt{\alpha_{WR}}} \left(1 - e^{-\alpha_{WR}t} \left(\frac{1 + \sqrt{\pi\alpha_{WR}t} - 2\sqrt{\alpha_{WR}t/\pi}}{1 + \sqrt{\pi\alpha_{WR}t} + (\pi - 2)\alpha_{WR}t}\right)\right) - \frac{c_2(1 - e^{-\alpha_{WR}t})}{\alpha_{WR}} \quad [9]$$

113 Figure 1 shows typical infiltration rates and cumulative infiltration curves of a silty clay loam  
 114 soil (Di Prima et al., 2020) and how the shapes of the curves change with different  $\alpha_{WR}$  values.  
 115 Clearly, the infiltration rates become attenuated as  $\alpha_{WR}$  values decrease, reflecting increased  
 116 effect of soil water repellency. The model also shows an increase followed by decrease of  
 117 infiltration rate for many  $\alpha_{WR}$  values, which reflects common observations of infiltration in  
 118 water repellent soils (e.g., Chen et al., 2020a; Imeson et al., 1992).



119

120 Figure 1: Ideal infiltration rate (upper panel) and cumulative infiltration (lower panel) curves

121 (dark full line) of a silty clay loam soil ( $S = 6 \text{ mm h}^{-1/2}$ , 10% saturation,  $A = 0.75 \text{ mm h}^{-1}$ )

122 respectively modeled by Equations [5] and [6] using data from Di Prima et al. (2020) and

123 synthetic variations of possible hydrophobic responses demonstrated by a range of  $\alpha_{WR}$  values

124 from 0.01 to 100 h<sup>-1</sup>.

## 125 **Materials and Methods**

126 We analyzed two datasets to test our model: one was collected following wildfires that occurred  
127 in the south-central Appalachian Mountains, USA, and the other was collected in four locations  
128 in Spain and France and assessed water repellency due to different inputs and in particular  
129 vegetation and fire effects.

### 130 *Wildfire study*

131 Data from 150 repeated tension infiltrometer experiments were used to assess the ability of  $\alpha_{WR}$   
132 to model the effect of hydrophobicity. The infiltration measurements were collected in burned  
133 vs. unburned sites in Mount Pleasant National Wildlife Refuge, Virginia, USA (37.73, -79.21),  
134 which experienced moderate to severe wildfires in November 2016. Here, we will refer to the  
135 sites as Burned 1 (41 experiments), Burned 2 (41 experiments), Unburned 1 (35 experiments),  
136 and Unburned 2 (33 experiments). The sites (Site 1 and Site 2) were on west-facing back slopes  
137 and shoulders. Within each site, infiltration tests occurred with spacing of 1-2 m between  
138 measurements. For each test, a mini-disk tension infiltrometer (Meter Group, Pullman,  
139 Washington, USA) was used with tension set to -1 cm. This tension was selected to ensure water  
140 flow occurred through all pores  $< 0.3$  cm in diameter (based on the Youngs-Laplace equation)  
141 while avoiding potential measurement errors associated with water entry into larger dead-end  
142 pores. Water volumes were recorded every 0.5 minutes, and continued for a minimum of 10  
143 readings. Measurements were collected on the following dates: 28 November 2016 (3 days after  
144 fire); 6 February 2017 (73 days after fire); 24 March 2017 (116 days after fire); 18 May 2017  
145 (171 days after fire); 27 June 2017 (211 days after fire); 22 August 2017 (267 days after fire); 3  
146 October 2017 (309 days after fire); and 4 December 2017 (371 days after fire).



147 Soil water repellency was measured at the same times and general locations as the infiltration  
148 tests. Here, water drop penetration time (WDPT) tests were conducted using an eye dropper. The  
149 soil or ash layer surface was cleared of any loose debris, and 5-7 drops were placed on the  
150 surface (0 cm depth). The time for the drops to infiltration was noted, with tests divided into two  
151 categories:  $WDPT < 10$  s versus  $WDPT \geq 10$  s (Chen et al., 2020a). The test was repeated at 10  
152 discrete locations within each sampling area. Water repellency was then quantified as the  
153 percentage of drops with  $WDPT \geq 10$  s over the total number of tests at a given sampling point.  
154 For more details, the reader is referred to Chen et al., (2020a) and Chen et al., (2020b).  
155 The three parameters ( $c_1$ ,  $c_2$ , and  $\alpha_{WR}$ ) were optimized for each infiltration test by minimizing  
156 the sum of square of errors (SSE) between measured and modeled cumulative infiltration. Note  
157 that we choose to fit cumulative infiltration (using Equation [9]) rather than infiltration rate  
158 because the former was better constrained at early times (with  $I = 0$  at  $t = 0$ ) and the measured  
159 cumulative infiltration data had less noise than the infiltration rate data.  
160 All 150 experiments were optimized with 41 sets of initial parameter values for  $c_1$ ,  $c_2$ , and  $\alpha_{WR}$ ,  
161 using all permutations of the following quantities:  $c_1 = 0.001, 0.01, 0.1, 1$  and  $10 \text{ cm min}^{-1/2}$ ;  $c_2 =$   
162  $0.001, 0.01, 0.1, 1$  and  $10 \text{ cm min}^{-1}$ , and  $\alpha_{WR} = 0.001, 0.01, 0.1, 1$  and  $10 \text{ min}^{-1}$ ). The parameter  
163 set with the smallest SSE was chosen as the global optimum solution. Cumulative histograms  
164 were developed for the optimized parameters ( $c_1$ ,  $c_2$ , and  $\alpha_{WR}$ ) under each of the four groups:  
165 Burned 1 (N=41), Burned 2 (N=41), Unburned 1 (N=35), and Unburned 2 (N=33). The  $\alpha_{WR}$   
166 values were also converted to  $t_{WR}$  using Equation [2], and the mean  $t_{WR}$  for each site and  
167 sampling date was compared to the corresponding water repellency.  
168 For comparison, we also analyzed the data using the two-term infiltration solution (Equation  
169 [3]), in this case optimizing for only  $c_1$  and  $c_2$ . The same initial parameter values were used for  $c_1$

170 and  $c_2$ , and again the global optimum set of values was identified for each test. The sum of  
171 square errors (SSE) from Equation [3] ( $SSE_{no\ \alpha}$ ) was then compared with SSE from Equation [9]  
172 ( $SSE_{\alpha}$ ).

173 We also evaluated if the parameter distributions varied between sites. Since all three parameters  
174 ( $c_1$ ,  $c_2$ , and  $\alpha_{WR}$ ) were non-normally distributed, even after log-transformation, we performed  
175 one-way Kruskal-Wallis tests for each parameter using site as the main factor. For any parameter  
176 with significant differences between sites, we performed a post-hoc Dunn test with the  
177 Benjamini-Hochberg method for p-value adjustments. We used a significance level (alpha) of  
178 0.05. Statistical analyses were conducted using R (version 4.0.3).

#### 179 *Vegetation-induced repellency study*

180 Fifteen infiltration experiments from three locations in Spain and France were also used to assess  
181 the effectiveness of Equation [9] compared to Equation [3]. Those experiments were divided as  
182 follows: 8 experiments from La Hunde site in Spain (Di Prima et al., 2017); 5 experiments from  
183 two locations in Django infiltration basin, France (Di Prima, Winiarski, et al., 2020 and  
184 unpublished data); and 2 experiments from ENTPE garden, in France (Concialdi et al., 2020).  
185 The infiltration tests were conducted using single ring infiltrometers with inner ring diameter of  
186 15 cm. For each test, the rings were inserted into the soil at a depth of ~1 cm. Slightly ponded  
187 conditions were maintained in the rings and the rate of water additions to the rings were recorded  
188 to determine infiltration rates. Soil physical properties of those sites spanned a wide spectrum of  
189 textural classes, as briefly described below.

190 The La Hunde site in Valencia, Spain (Di Prima et al., 2017) consisted of two contiguous plots,  
191 each of 1800 m<sup>2</sup>, located at the headwaters of Rambla Espadilla catchment within the public  
192 forest La Hunde (39°4'50'' N, 1°14'47'' W, elevation of 1090 m a.s.l.), Valencia (NE Spain).

193 Plots were located in a typical Mediterranean oak forest approximately 60 years old,  
194 characterized by *Quercus ilex* sbsp. *ballota* in association with other xerophytic species such as  
195 *Pinus halepensis*, *Quercus faginea*, *Juniperus phoenicea* and *Juniperus oxycedrus*. The climate  
196 was Mediterranean with a mean annual rainfall of 466 mm and a mean annual temperature of  
197 13.7 °C (1960–2007). According to the USDA standards, the soil of the studied area was  
198 classified as clay loam. The soil was approximately 30-50 cm deep in the lower part of the slope  
199 and about 10 cm thick in higher elevations, with rock fragments constituting up to 50% of the  
200 soil volume (del Campo et al., 2019).

201 The Django site occurred within a stormwater infiltration basin, named Django Reinhardt basin,  
202 located in Chassieu in the eastern suburbs of Lyon, France (Di Prima, Winiarski, et al., 2020). A  
203 detailed description of the experimental area can be found in Goutaland et al. (2008) and  
204 Winiarski et al. (2006). The infiltration basin was constructed above a heterogeneous  
205 glaciofluvial deposit by mixing the top 50–80 cm of the soil. The coarse glaciofluvial deposit  
206 was composed of four main lithofacies: i) the upper sandy layer that was a mixture of the soil  
207 matrix and gravel, ii) a mixture of the soil matrix and gravel with a bimodal particle size  
208 distribution that occupied most of the deposit below the top 50–80 cm layer, iii) large lenses of  
209 sand, and iv) smaller lenses of matrix-free gravel (Ben Slimene et al., 2017; Goutaland et al.,  
210 2013). At surface, a sedimentary layer was deposited with high contents of organic matter,  
211 impeding water infiltration at the basin scale (Lassabatere et al., 2010). The high organic  
212 contents resulted from both vegetation and pollutants loads brought by the entering stormwater  
213 (Badin et al., 2008).

214 The ENTPE site in Lyon, France (Concialdi et al., 2020) contained a sandy loam soil located in  
215 the garden of the École Nationale des Travaux Publics de l'État (ENTPE) in the municipality of

216 Vaulx-en-Velin (France). The site was chosen to represent a typical rain garden developed to  
217 restore hydrological processes (i.e., water infiltration capacity) in urban areas.

218

## 219 **Results and Discussion**

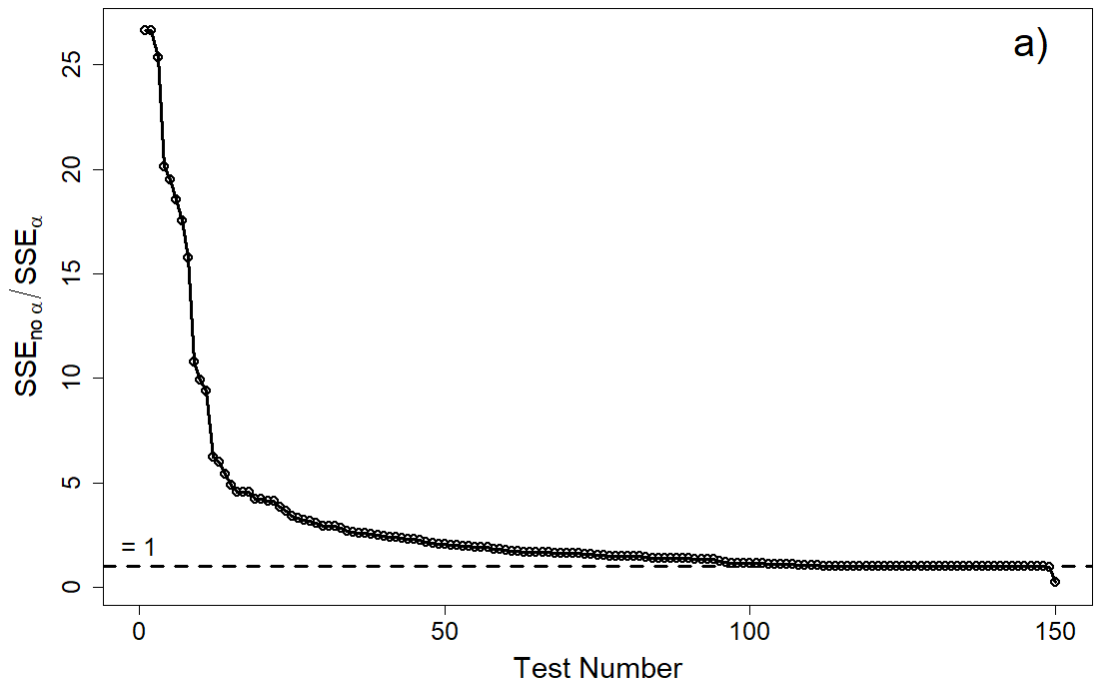
### 220 *Wildfire induced water repellency*

221 The proposed model (Equation [1], approximated for the two-parameter model by Equation [9])  
222 provided better fits to measured data compared to the standard infiltration model (Equation [3])  
223 for most of the measurements (Figure 2). Specifically, the ratio of  $SSE_{no\ \alpha}/SSE_{\alpha}$  was greater than  
224 1 for 116 out of 150 infiltration tests, and was less than 1 for only 2 out of 150 infiltration tests  
225 (Figure 2a). Equation [9] improved the model fit more in burned compared to unburned soils, as  
226 difference in SSE between Equation [3] ( $SSE_{no\ \alpha}$ ) versus Equation [9] ( $SSE_{\alpha}$ ) was larger for the  
227 former (Figure 2b).

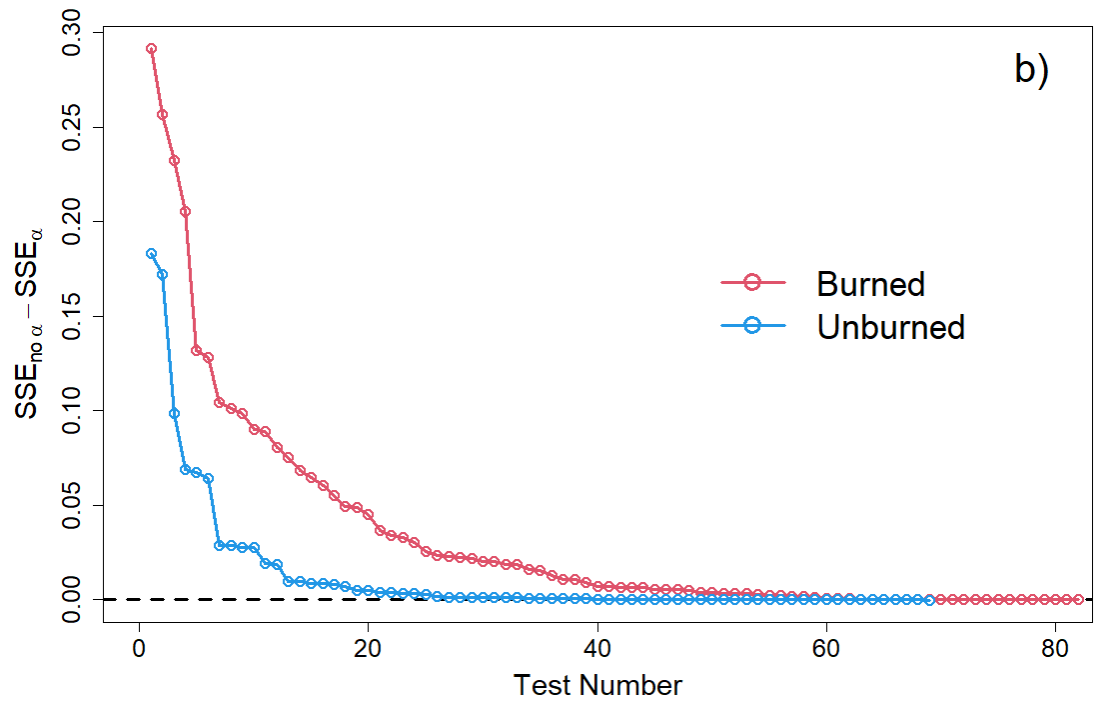
228 The cumulative histograms of parameter values for the wildfire study (Figure 3) showed that  
229 both burned areas (Burned 1 and Burned 2) had smaller median  $\alpha_{WR}$  values than the unburned  
230 areas (Unburned 1 and Unburned 2). The Kruskal-Wallis test indicated that  $\alpha_{WR}$  distributions  
231 were significantly different between sites ( $p = 0.0011$ ), and the post-hoc Dunn test revealed that  
232 the Burned 2 site had significantly smaller  $\alpha_{WR}$  values than the other three sites ( $0.003 < p <$   
233  $0.028$ ). That site experienced the greatest burn severity (Chen et al., 2020a) and in general had  
234 the strongest water repellency at the surface (Chen et al., 2020b). Since smaller values of  $\alpha_{WR}$   
235 correspond to longer-lasting water repellency (as shown in Figure 1), this result indicates that the  
236  $\alpha_{WR}$  parameter successfully adjusted the infiltration model to fit to hydrophobic conditions.  
237 Furthermore, Figure 3 also shows that the  $c_1$  and  $c_2$  parameters did not show substantial  
238 differences in their distributions between burned and unburned sites, Those results were further

239 supported by the Kruskal-Wallis tests, which determined that  $c_1$  and  $c_2$  did not significantly  
240 differ between sites ( $p > 0.05$ ). Taken together, these findings suggest the fires may not have  
241 induced permanent changes in soil hydraulic properties (e.g., sorptivity, hydraulic conductivity),  
242 and moreover that the proposed scaling factor can account for transient changes to those  
243 properties due to soil water repellency. Nonetheless, additional tests, such as laboratory  
244 characterization, would be necessary to fully support or refute this hypothesis.

245 We also separated the infiltration measurements based on the relative water repellency measured  
246 on each sampling date. Specifically, measurements were grouped into those that occurred when  
247 50% or more of the WDPT tests were less than 10 s (i.e., water repellency  $\leq 50\%$ ) and those that  
248 occurred when the majority of WDPT tests exceeded 10 s (i.e., water repellency  $> 50\%$ ). The  $t_{WR}$   
249 values were consistently higher for tests conducted when the soil was more water-repellent  
250 (Figure 4). For example,  $t_{WR}$  was greater than 0.1 minutes for about 80% of tests conducted when  
251 water repellency exceeded 50%, whereas only about 40% of tests under low water repellency  
252 had  $t_{WR}$  values greater than 0.1 minutes. These results imply that the magnitude of  $t_{WR}$  may be  
253 related to soil water repellency, providing some support to our initial hypothesis. However,  
254 future studies should explore this relationship more carefully, for example by measuring water  
255 repellency in direct conjunction with infiltration (Tillman et al., 1989).



256



257

258

259

260

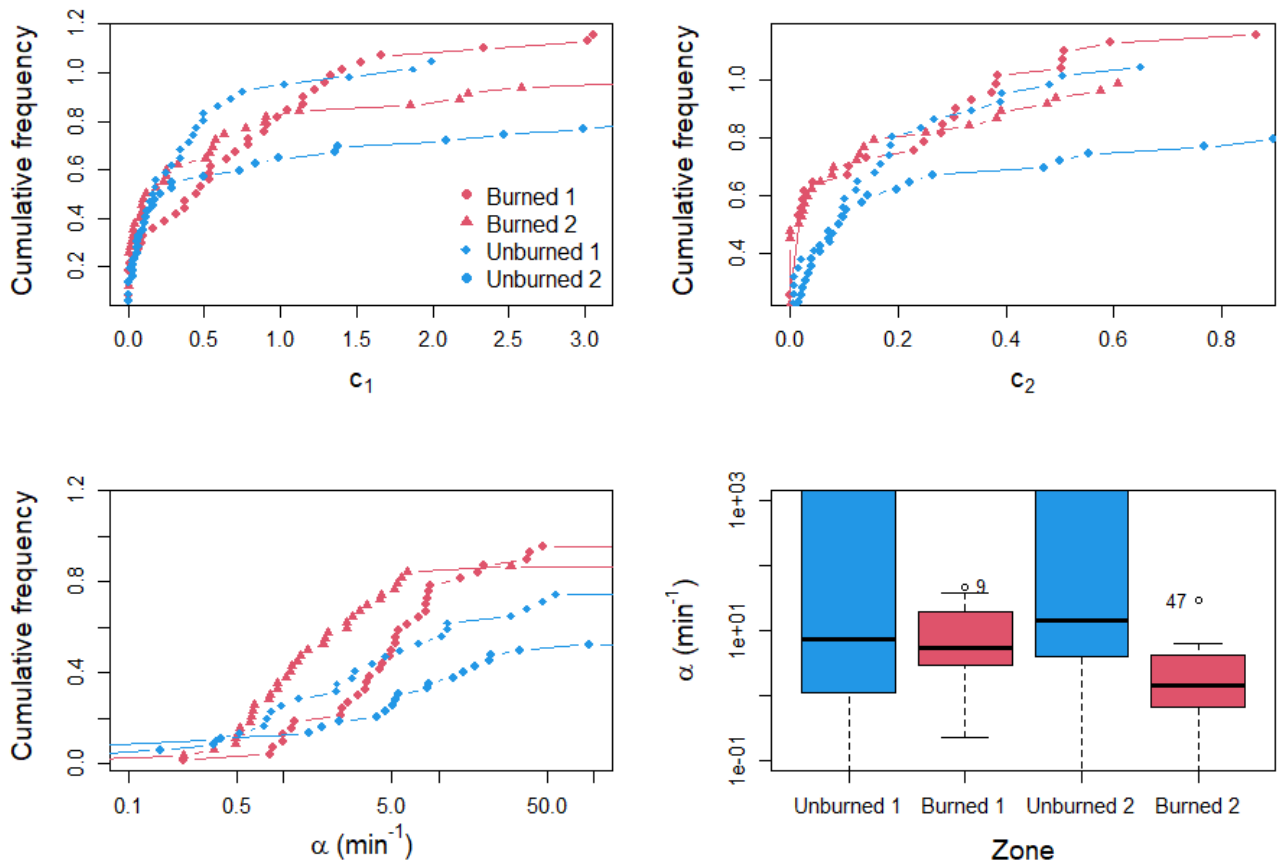
261

Figure 2: Upper panel shows ratios of SSE values ( $SSE_{no \alpha} / SSE_{\alpha}$ ) and lower panel shows

differences ( $SSE_{no \alpha} - SSE_{\alpha}$ ) between Equation [3] (no  $\alpha_{WR}$ ) and Equation [9] (with  $\alpha_{WR}$ ) for the

150 infiltration experiments from two burned and unburned areas. Note that the runs are

organized in decreasing order in each panel.



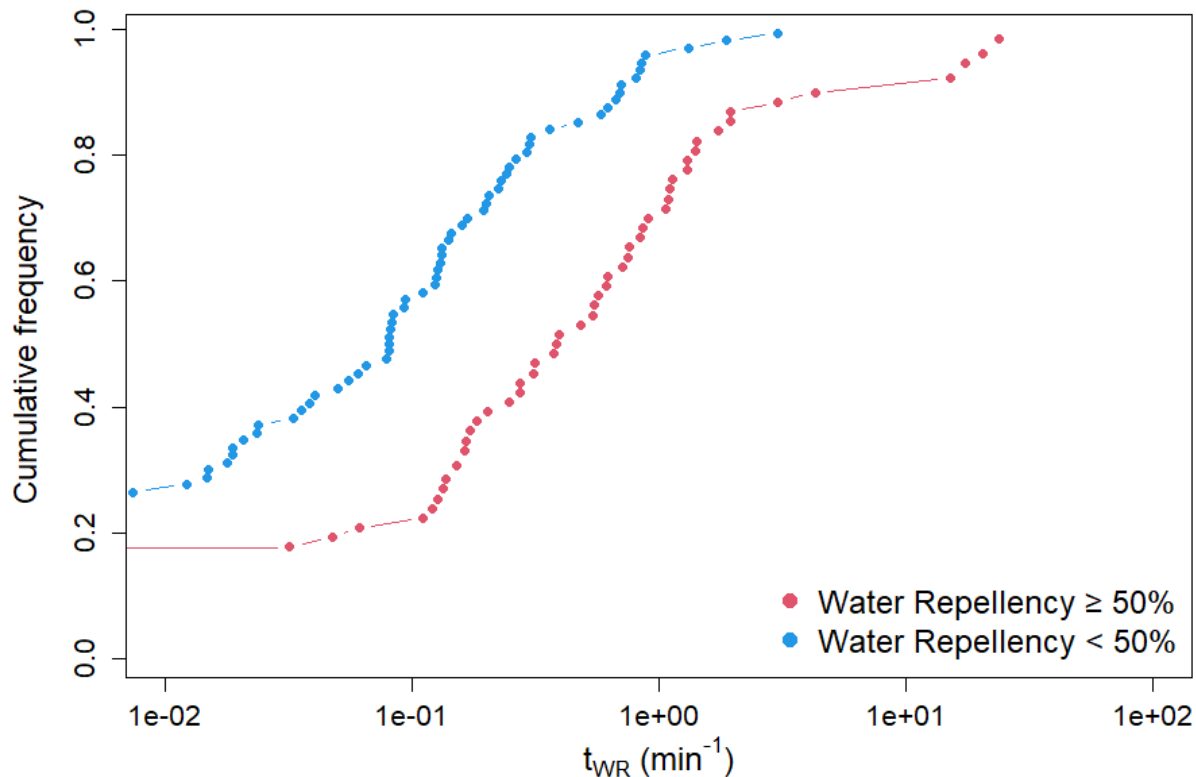
263

264

265

266

Figure 3: Cumulative histogram for  $\alpha_{WR}$  (min<sup>-1</sup>),  $c_1$  (cm min<sup>-1/2</sup>), and  $c_2$  (cm min<sup>-1</sup>) for the 150 infiltration experiments from two burned and unburned areas, box plot of the distributions for  $\alpha_{WR}$  (min<sup>-1</sup>) for the four zones (sites 1 and 2, burned and unburned zones).



267  
 268 Figure 4: Cumulative frequency distributions for characteristic water repellency time,  $t_{WR}$  (min),  
 269 for infiltration measurements collected when the surface soils exhibited low ( $\leq 50\%$ ) or high (>  
 270 50%) water repellency, as assessed using multiple water drop penetration time tests.

271  
 272 *Vegetation-induced water repellency*

273 In the study of vegetation-induced repellency, Equation [9] gave better fits to observations (i.e.,  
 274  $SSE_{no\ \alpha}/SSE_{\alpha} > 1$ ) for 14 out of 15 infiltration experiments (Table 1 and Figure 5). The remaining  
 275 site showed no change (i.e.,  $SSE_{no\ \alpha}/SSE_{\alpha} = 1$ ), possibly due to limited effect of water repellency  
 276 in those instances. Using Equation [9] also resulted in the  $c_1$  parameter being  $> 0$  for all but four  
 277 infiltration experiments. In contrast,  $c_1 = 0$  was obtained for 14 out of 15 infiltration tests when  
 278 the uncorrected Equation [3] was used. Since  $c_1$  is often considered to represent soil sorptivity



279 (Stewart & Abou Najm, 2018a, 2018b), values of 0 are only physically plausible in saturated  
280 conditions. Future studies should consider whether the use of Equation [9] can be used to  
281 accurately constrain hydraulic parameters such as sorptivity and hydraulic conductivity from  
282 infiltration tests conducted in water-repellent soils.

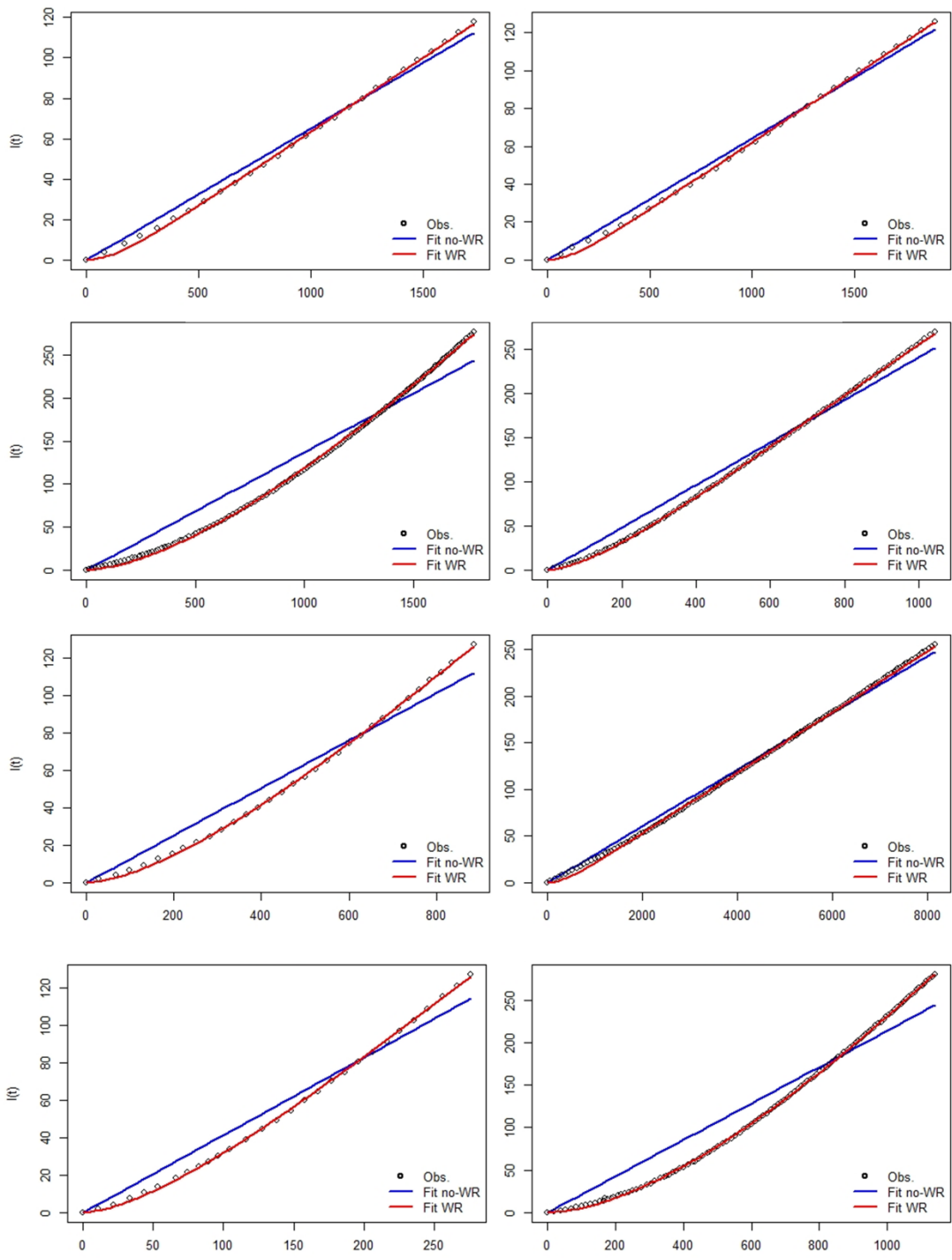
283 The need for new approaches to deal with infiltration into water-repellent soils has been  
284 discussed in previous studies. For instance, the BEST methods that were used for the  
285 characterization of soil water retention and hydraulic conductivity functions currently only apply  
286 to concave curves (Angulo-Jaramillo et al., 2019), and not the convex curves typical of water-  
287 repellent soils. With our model, and its time-dependent water repellency term ( $1 - e^{-\alpha_{WR}t}$ ), we  
288 can now deduce unscaled cumulative infiltration (i.e., infiltration driven by capillarity and  
289 gravity without water repellency) from Equation [1]:

$$290 \quad i(t) = \frac{i_{WR}(t)}{(1 - e^{-\alpha_{WR}t})} \quad [11].$$

291 The integration of the corrected infiltration rate  $i(t)$  will provide the corresponding corrected  
292 cumulative infiltration rate. Using this approach may make it possible use BEST or other  
293 algorithms and derive soil hydraulic parameters from convex cumulative infiltration curves. At  
294 the same time, the relative consistency of hydraulic parameters  $c_1$  and  $c_2$  identified in the wildfire  
295 study (Figure 3) suggests that this approach may assist in a complete characterization of  
296 hydrophobic soils. We note, however, that additional measurements (e.g., WDPTs) may still be  
297 required, particularly since models modified with the correction term may suffer from  
298 equifinality or related sources of uncertainty when fit solely to infiltration data. This topic should  
299 be the subject of further research.

300 Table 1: Results from 15 infiltration experiments demonstrating the effectiveness of proposed exponential scaling factor  $(1 - e^{-\alpha_{WR}t})$   
 301 by comparing Equation [3] with Equation [9].

<i>Site</i>	<i>Reference</i>	<i>Run</i>	Eq. 3			Eq. 9				$SSE_{no\ a}/SSE_a$
			$c_1$	$c_2$	$SSE_{no\ a}$	$c_1$	$c_2$	$\alpha_{WR}$	$SSE_a$	
La Hunde (Spain)	Di Prima et al. (2017)	5	0.00	0.19	836	5.79	0.10	0.006	170	4.89
		14	0.00	0.14	640	5.45	0.07	0.004	192	3.33
		2	0.00	0.24	721	7.17	0.13	0.006	41	17.76
		16	0.00	0.26	459	0.00	0.30	0.027	61	7.44
		13	0.00	0.09	780	4.86	0.05	0.002	123	6.32
		18	1.19	0.33	45	1.19	0.33	>100	45	1.00
		1	0.00	0.41	1515	11.82	0.30	0.007	31	48.31
		11	0.00	0.19	549	0.00	0.22	0.020	61	8.96
Django (France)	Di Prima et al. (2020b)	34	0.00	0.24	13404	10.08	0.14	0.003	1036	130.09
		10	0.00	0.14	53264	9.45	0.17	0.001	681	78.16
		40	0.00	0.21	56274	7.43	0.35	0.001	159	353.23
		75	0.00	0.13	1962	6.18	0.12	0.002	33	59.34
		76	0.00	0.28	1514	9.42	0.12	0.005	58	26.02
ENTPE-1 (France)	Concialdi et al. (2020)	4	0.00	0.02	938	0.00	0.02	0.005	270	3.47
		8	0.00	0.03	3465	0.00	0.03	0.003	431	8.03



303

304

Figure 5: Examples from each of the three locations comparing experimental results from  
 305 infiltration experiments (circles) to results from Equation [3] (blue) and Equation [9] (red).

306

307 **Conclusion**

308 An exponential scaling factor ( $1 - e^{-\alpha_{WR}t}$ ) was proposed to model the effect of water  
309 repellency and hydrophobicity in infiltration models. The model contains one additional  
310 parameter ( $\alpha_{WR}$ ), which can be considered to reflect the rate at which water repellency  
311 diminishes during infiltration. Though empirical in nature,  $\alpha_{WR}$  can be used to derive a  
312 characteristic time,  $t_{WR}$ , at which infiltration rates recover to some percentage (e.g., 50%) of  
313 infiltration under non-repellent conditions. The time  $t_{WR}$  may be considered as a characteristic  
314 time for water repellency, and therefore may be comparable with other types of characteristics  
315 times such as water drop penetration test (WDPT) times.

316 Results for 165 infiltration experiments – representing different ecosystems with a variety of  
317 sources and levels of soils water repellency – were used to demonstrate the effectiveness of this  
318 simple method to characterize water repellency in infiltration models. For example, the analysis  
319 showed that  $\alpha_{WR}$  has smaller values in soils that were burned during a wildfire compared to  
320 unburned controls. The magnitude of  $t_{WR}$  also had some correlation with the amount of water  
321 repellency measured at the time of infiltration, suggesting that it may be useful as a way to  
322 characterize the degree and persistence of soil water repellency.

323 Even though we focused our comparisons on variations of a widely used two-term infiltration  
324 equation, the scaling factor can be applied to any infiltration model. In addition, the proposed  
325 approach could be combined with other approaches to offer the complete determination of soil  
326 hydraulic properties, including hydrophobicity. Future work may therefore consider questions  
327 such as whether the  $\alpha$  parameter can be predicted based on other indicators (e.g., WDPT times)  
328 and if it can provide a consistent measure for both the degree and duration of water repellency.

329

330 **Data Availability Statement**

331 Dr. Jingjing Chen led the field measurements for the wildfire study. Data is available through J.  
332 Chen et al., (2020a); J. Chen et al., (2020b); Di Prima et al., (2017); Di Prima et al., (2020); and  
333 Concialdi et al., (2020) ) and are summarized in a zip file containing all.csv and. r files used in  
334 the Supplement Files (WRR\_Infiltration\_correction\_Data.zip). Data are also available and will  
335 be permanently archived at <https://data.lib.vt.edu/files/3197xm23r>.

336

337 **Acknowledgments**

338 The authors would like to acknowledge the helpful suggestions from Professor Teamrat  
339 Ghezzehei, who suggested to consider applying the scaling factor to the infiltration rate instead  
340 of cumulative infiltration. Funding for this work was provided in part by the University of  
341 California–Davis, Agricultural Experiment Station, the Virginia Agricultural Experiment Station  
342 and the Multistate Hatch Program W4188 of the USDA, National Institute of Food and  
343 Agriculture. This work was also supported through the INFILTRON Project (ANR-17-CE04-  
344 0010, Package for assessing infiltration & filtration functions of urban soils in stormwater  
345 management; <https://infiltron.org/>) funded by the French National Research Agency (ANR).

346

347 **Reference**

- 348 Adams, R. H., Guzmán Osorio, F. J., & Zavala Cruz, J. (2008). Water repellency in oil  
349 contaminated sandy and clayey soils. *International Journal of Environmental Science &*  
350 *Technology*, 5(4), 445–454. <https://doi.org/10.1007/BF03326040>
- 351 Angulo-Jaramillo, R., Bagarello, V., Di Prima, S., Gosset, A., Iovino, M., & Lassabatere, L.  
352 (2019). Beerkan Estimation of Soil Transfer parameters (BEST) across soils and scales.  
353 *Journal of Hydrology*, 576, 239–261. <https://doi.org/10.1016/j.jhydrol.2019.06.007>
- 354 Arye, G., Tarchitzky, J., & Chen, Y. (2011). Treated wastewater effects on water repellency and  
355 soil hydraulic properties of soil aquifer treatment infiltration basins. *Journal of*  
356 *Hydrology*, 397(1–2), 136–145. <https://doi.org/10.1016/j.jhydrol.2010.11.046>
- 357 Badin, A.-L., Faure, P., Bedell, J.-P., & Delolme, C. (2008). Distribution of organic pollutants  
358 and natural organic matter in urban storm water sediments as a function of grain size.  
359 *Science of The Total Environment*, 403(1–3), 178–187.  
360 <https://doi.org/10.1016/j.scitotenv.2008.05.022>
- 361 Bauters, T. W. J., Steenhuis, T. S., DiCarlo, D. A., Nieber, J. L., Dekker, L. W., Ritsema, C. J., et  
362 al. (2000). Physics of water repellent soils. *Journal of Hydrology*, 231–232, 233–243.  
363 [https://doi.org/10.1016/S0022-1694\(00\)00197-9](https://doi.org/10.1016/S0022-1694(00)00197-9)
- 364 Ben Slimene, E., Lassabatere, L., Šimůnek, J., Winiarski, T., & Gourdon, R. (2017). The role of  
365 heterogeneous lithology in a glaciofluvial deposit on unsaturated preferential flow – a  
366 numerical study. *Journal of Hydrology and Hydromechanics*, 65(3), 209–221.  
367 <https://doi.org/10.1515/johh-2017-0004>
- 368 del Campo, A. D., González-Sanchis, M., García-Prats, A., Ceacero, C. J., & Lull, C. (2019).  
369 The impact of adaptive forest management on water fluxes and growth dynamics in a

370 water-limited low-biomass oak coppice. *Agricultural and Forest Meteorology*, 264, 266–  
371 282. <https://doi.org/10.1016/j.agrformet.2018.10.016>

372 Chen, J., McGuire, K. J., & Stewart, R. D. (2020a). Effect of soil water-repellent layer depth on  
373 post-wildfire hydrological processes. *Hydrological Processes*, 34(2), 270–283.  
374 <https://doi.org/10.1002/hyp.13583>

375 Chen, J., Pangle, L. A., Gannon, J. P., & Stewart, R. D. (2020b). Soil water repellency after  
376 wildfires in the Blue Ridge Mountains (in press). *Soil Water Repellency after Wildfires in*  
377 *the Blue Ridge Mountains*.

378 Chen, L., Berli, M., & Chief, K. (2013). Examining Modeling Approaches for the Rainfall-  
379 Runoff Process in Wildfire-Affected Watersheds: Using San Dimas Experimental Forest.  
380 *JAWRA Journal of the American Water Resources Association*, 49(4), 851–866.  
381 <https://doi.org/10.1111/jawr.12043>

382 Concialdi, P., Di Prima, S., Bhanderi, H. M., Stewart, R. D., Abou Najm, M. R., Lal Gaur, M., et  
383 al. (2020). An open-source instrumentation package for intensive soil hydraulic  
384 characterization. *Journal of Hydrology*, 582.  
385 <https://doi.org/10.1016/j.jhydrol.2019.124492>

386 DeBano, L. F., Mann, L. D., & Hamilton, D. A. (1970). Translocation of Hydrophobic  
387 Substances into Soil by Burning Organic Litter. *Soil Science Society of America Journal*,  
388 34(1), 130–133. <https://doi.org/10.2136/sssaj1970.03615995003400010035x>

389 Dekker, L. W., Doerr, S. H., Oostindie, K., Ziogas, A. K., & Ritsema, C. J. (2001). Water  
390 Repellency and Critical Soil Water Content in a Dune Sand. *Soil Science Society of*  
391 *America Journal*, 65(6), 1667. <https://doi.org/10.2136/sssaj2001.1667>

392 Di Prima, S., Bagarello, V., Angulo-Jaramillo, R., Bautista, I., Cerdà, A., del Campo, A., et al.  
393 (2017). Impacts of thinning of a Mediterranean oak forest on soil properties influencing  
394 water infiltration. *Journal of Hydrology and Hydromechanics*, 65(3), 276–286.  
395 <https://doi.org/10.1515/johh-2017-0016>

396 Di Prima, S., Castellini, M., Majdi R. Abou Najm, Stewart, R. D., Angulo-Jaramillo, R.,  
397 Winiarski, T., & Lassabatere, L. (2019). Experimental assessment of a new  
398 comprehensive model for single ring infiltration data. *Journal of Hydrology*, 573, 937–  
399 951. <https://doi.org/10.1016/j.jhydrol.2019.03.077>

400 Di Prima, S., Winiarski, T., Angulo-Jaramillo, R., Stewart, R. D., Castellini, M., Abou Najm, M.  
401 R., et al. (2020). Detecting infiltrated water and preferential flow pathways through time-  
402 lapse ground-penetrating radar surveys. *Science of The Total Environment*, 138511.  
403 <https://doi.org/10.1016/j.scitotenv.2020.138511>

404 Di Prima, S., Stewart, R. D., Castellini, M., Bagarello, V., Abou Najm, M. R., Pirastru, M., et al.  
405 (2020). Estimating the macroscopic capillary length from Beerkan infiltration  
406 experiments and its impact on saturated soil hydraulic conductivity predictions. *Journal*  
407 *of Hydrology*, 589, 125159. <https://doi.org/10.1016/j.jhydrol.2020.125159>

408 Doerr, S. H., & Thomas, A. D. (2000). The role of soil moisture in controlling water repellency:  
409 new evidence from forest soils in Portugal. *Journal of Hydrology*, 231–232, 134–147.  
410 [https://doi.org/10.1016/S0022-1694\(00\)00190-6](https://doi.org/10.1016/S0022-1694(00)00190-6)

411 Doerr, S. H., Shakesby, R. A., Blake, W. H., Chafer, C. J., Humphreys, G. S., & Wallbrink, P. J.  
412 (2006). Effects of differing wildfire severities on soil wettability and implications for  
413 hydrological response. *Journal of Hydrology*, 319(1), 295–311.  
414 <https://doi.org/10.1016/j.jhydrol.2005.06.038>



415 Ebel, B. A., & Moody, J. A. (2020). Parameter estimation for multiple post-wildfire hydrologic  
416 models. *Hydrological Processes*, n/a(n/a). <https://doi.org/10.1002/hyp.13865>

417 Ebel, B. A., Moody, J. A., & Martin, D. A. (2012). Hydrologic conditions controlling runoff  
418 generation immediately after wildfire. *Water Resources Research*, 48(3), W03529.  
419 <https://doi.org/10.1029/2011WR011470>

420 Ebel, B. A., Rengers, F. K., & Tucker, G. E. (2016). Observed and simulated hydrologic  
421 response for a first-order catchment during extreme rainfall 3 years after wildfire  
422 disturbance. *Water Resources Research*, 52(12), 9367–9389.  
423 <https://doi.org/10.1002/2016WR019110>

424 Goutaland, D., Winiarski, T., Lassabatere, L., Dubé, J. S., & Angulo-Jaramillo, R. (2013).  
425 Sedimentary and hydraulic characterization of a heterogeneous glaciofluvial deposit:  
426 Application to the modeling of unsaturated flow. *Engineering Geology*, 166, 127–139.  
427 <https://doi.org/10.1016/j.enggeo.2013.09.006>

428 Goutaland, David, Winiarski, T., Dubé, J.-S., Bièvre, G., Buoncristiani, J.-F., Chouteau, M., &  
429 Giroux, B. (2008). Hydrostratigraphic Characterization of Glaciofluvial Deposits  
430 Underlying an Infiltration Basin Using Ground Penetrating Radar. *Vadose Zone Journal*,  
431 7(1), 194. <https://doi.org/10.2136/vzj2007.0003>

432 Hewelke, E., Szatyłowicz, J., Hewelke, P., Gnatowski, T., & Aghalarov, R. (2018). The Impact  
433 of Diesel Oil Pollution on the Hydrophobicity and CO<sub>2</sub> Efflux of Forest Soils. *Water,*  
434 *Air, & Soil Pollution*, 229(2), 51. <https://doi.org/10.1007/s11270-018-3720-6>

435 Imeson, A. C., Verstraten, J. M., van Mulligen, E. J., & Sevink, J. (1992). The effects of fire and  
436 water repellency on infiltration and runoff under Mediterranean type forest. *CATENA*,  
437 19(3–4), 345–361. [https://doi.org/10.1016/0341-8162\(92\)90008-Y](https://doi.org/10.1016/0341-8162(92)90008-Y)

438 Lassabatere, L., Angulo-Jaramillo, R., Goutaland, D., Letellier, L., Gaudet, J. P., Winiarski, T.,  
439 & Delolme, C. (2010). Effect of the settlement of sediments on water infiltration in two  
440 urban infiltration basins. *Geoderma*, 156(3–4), 316–325.  
441 <https://doi.org/10.1016/j.geoderma.2010.02.031>

442 Li, Y., Ren, X., Hill, R., Malone, R., & Zhao, Y. (2018). Characteristics of Water Infiltration in  
443 Layered Water-Repellent Soils. *Pedosphere*, 28(5), 775–792.  
444 [https://doi.org/10.1016/S1002-0160\(17\)60414-4](https://doi.org/10.1016/S1002-0160(17)60414-4)

445 Lichner, L., Felde, V. J. M. N. L., Büdel, B., Leue, M., Gerke, H. H., Ellerbrock, R. H., et al.  
446 (2018). Effect of vegetation and its succession on water repellency in sandy soils.  
447 *Ecohydrology*, 11(6), e1991. <https://doi.org/10.1002/eco.1991>

448 Mansell, R. S. (1970). Infiltration of water into soil columns which have a water-repellent layer.  
449 In *Soil Crop Sci Soc Fla Proc*.

450 McGuire, L. A., Rengers, F. K., Kean, J. W., Staley, D. M., & Mirus, B. B. (2018). Incorporating  
451 spatially heterogeneous infiltration capacity into hydrologic models with applications for  
452 simulating post-wildfire debris flow initiation. *Hydrological Processes*, 32(9), 1173–  
453 1187. <https://doi.org/10.1002/hyp.11458>

454 Moody, J. A., Martin, R. G., & Ebel, B. A. (2019). Sources of inherent infiltration variability in  
455 postwildfire soils. *Hydrological Processes*, 33(23), 3010–3029.  
456 <https://doi.org/10.1002/hyp.13543>

457 Philip, J. R. (1957). The infiltration equation and its solution. *Soil Science*, 83(5).  
458 <https://doi.org/10.1097/00010694-195705000-00002>

459 Philip, J.-R. (1969). Theory of infiltration. In *Advances in hydroscience* (Vol. 5, pp. 215–296).  
460 Elsevier.

461 Rengers, F. K., McGuire, L. A., Kean, J. W., Staley, D. M., & Youberg, A. M. (2019). Progress  
462 in simplifying hydrologic model parameterization for broad applications to post-wildfire  
463 flooding and debris-flow hazards. *Earth Surface Processes and Landforms*, 44(15),  
464 3078–3092. <https://doi.org/10.1002/esp.4697>

465 Robichaud, P. R. (2000). Fire effects on infiltration rates after prescribed fire in Northern Rocky  
466 Mountain forests, USA. *Journal of Hydrology*, 231, 220–229.

467 Roy, J. L., & McGill, W. B. (2000). Investigation into mechanisms leading to the development,  
468 spread and persistence of soil water repellency following contamination by crude oil.  
469 *Canadian Journal of Soil Science*, 80(4), 595–606. <https://doi.org/10.4141/S99-091>

470 Rye, C. F., & Smettem, K. R. J. (2017). The effect of water repellent soil surface layers on  
471 preferential flow and bare soil evaporation. *Geoderma*, 289, 142–149.  
472 <https://doi.org/10.1016/j.geoderma.2016.11.032>

473 Stavi, I., & Rosenzweig, R. (2020). Tillage effect on hydrophobicity and hydrological properties  
474 of oil-contaminated sediments in a hyper-arid region. *Arid Land Research and*  
475 *Management*, 34(1), 26–35. <https://doi.org/10.1080/15324982.2019.1599468>

476 Stewart, R. D., & Abou Najm, M. R. (2018a). A Comprehensive Model for Single Ring  
477 Infiltration I: Initial Water Content and Soil Hydraulic Properties. *Soil Science Society of*  
478 *America Journal*, 82(3), 548–557. <https://doi.org/10.2136/sssaj2017.09.0313>

479 Stewart, R. D., & Abou Najm, M. R. (2018b). A Comprehensive Model for Single Ring  
480 Infiltration II: Estimating Field-Saturated Hydraulic Conductivity. *Soil Science Society of*  
481 *America Journal*, 82(3), 558–567. <https://doi.org/10.2136/sssaj2017.09.0314>

482 Tillman, R. W., Scotter, D. R., Wallis, M. G., & Clothier, B. E. (1989). Water repellency and its  
483 measurement by using intrinsic sorptivity. *Soil Research*, 27(4), 637–644.

484 Vandervaere, J. P., Vauclin, M., & Elrick, D. E. (2000a). Transient flow from tension  
485 infiltrmeters: I. The two-parameter equation. *SoilScience Society of America Journal*,  
486 64(4), 1263–1272. <https://doi.org/10.2136/sssaj2000.6441263x>

487 Vandervaere, J. P., Vauclin, M., & Elrick, D. E. (2000b). Transient flow from tension  
488 infiltrmeters: II. Four methods to determine sorptivityand conductivity. *Soil Science*  
489 *Society of America Journal*, 64(4), 1272–1284.  
490 <https://doi.org/10.2136/sssaj2000.6441272x>

491 Winiarski, T., Bedell, J.-P., Delolme, C., & Perrodin, Y. (2006). The impact of stormwater on a  
492 soil profile in an infiltration basin. *Hydrogeology Journal*, 14(7), 1244–1251.  
493 <https://doi.org/10.1007/s10040-006-0073-9>

494